Skewless Network Clock Synchronization Without Discontinuity: Convergence and Performance

Enrique Mallada*, Xiaoqiao Meng†, Michel Hack†, Li Zhang†, and Ao Tang*
* School of ECE, Cornell University, Ithaca, NY 14853, USA.
† IBM T. J. Watson Research Center. 1101 Kitchawan Rd, Yorktown Heights, NY 10598, USA.

***Abstract*—This paper examines synchronization of computer clocks connected via a data network and proposes a skewless algorithm to synchronize them. Unlike existing solutions, which either estimate and compensate the frequency difference (skew) among clocks or introduce offset corrections that can generate jitter and possibly even backward jumps, our solution achieves synchronization without these problems. We first analyze the convergence property of the algorithm and provide explicit necessary and sufficient conditions on the parameters to guarantee synchronization. We then study the effect of noisy measurements (jitter) and frequency drift (wander) on the offsets and synchronization frequency, and further optimize the parameter values to minimize their variance. Our study reveals a few insights, for example, we show that our algorithm can converge even in the presence of timing loops and noise, provided that there is a well defined leader. This marks a clear contrast with current standards such as NTP and PTP, where timing loops are specifically avoided. Furthermore, timing loops can even be beneficial in our scheme as it is demonstrated that highly connected subnetworks can collectively outperform individual clients when the time source has large jitter. The results are supported by experiments running on a cluster of IBM BladeCenter servers with Linux.**

I. Introduction

Keeping consistent time among different nodes in a network is a fundamental requirement of many distributed applications. Nodes' internal clocks are usually not accurate enough and tend to drift apart from each other over time, generating inconsistent time values. Network clock synchronization allows these devices to correct their clocks to match a global reference of time, such as the Universal Coordinated Time (UTC), by performing time measurements through a network. For example, for the Internet, network clock synchronization has been an important subject of research and several different protocols have been proposed [2]–[8]. These protocols are used for various applications with diverse precision requirements such as banking transactions, communications, traffic measurement and security protection. For example, in modern wireless cellular networks, time-sharing protocols need an accuracy of several microseconds to guarantee the efficient use of channel capacity. Another example is the recently announced Google Spanner [9], a globally-distributed database, which depends on globally-synchronized clocks within at most several milliseconds drifts.

The current *de facto* standard for IP networks is the Network Time Protocol (NTP) proposed by David Mills [2]. It is a low-cost, purely software-based solution whose accuracy mostly ranges from hundreds of microseconds to several milliseconds. On the other hand, IEEE 1588 (PTP) [4] gives superior performance by achieving sub-microsecond or even nanosecond accuracy. However, it is relatively expensive as it requires special hardware support to achieve those accuracy levels and may not be fully compatible with legacy cluster systems.

Newer synchronization protocols have been proposed with the objective of balancing between accuracy and cost. For example, IBM Coordinated Cluster Time (CCT) [10] is able to provide better performance than NTP without additional hardware. Its success is based on a skew estimation mechanism [11] that progressively adapts the clock frequency without offset corrections. Another alternative is the RADclock [5], [8] which estimates the skew and produces offset corrections, but provides a secondary relative clock that is more robust to jitter.

There are two major difficulties that make the network clock synchronization problem challenging. Firstly, the frequency of hardware clocks is sensitive to temperature and is constantly varying. Secondly, the latency introduced by the OS and network congestion delay results in errors in the time measurements which can be propagated through the network. Thus, most protocols introduce different ways of estimating the frequency mismatch (skew) [11], [12] and measuring the time difference (offset) [13], [14] while maintaining a simple network topology [2], [4]. This leads in particular to extensive literature on skew estimation [12], [15]–[17] which suggests that explicit skew estimation is necessary for clock synchronization.

This paper takes a different approach and shows that focusing on skew estimation could be misleading. We provide a simple algorithm that is able to compensate the clock skew without any explicit estimation of it. Our algorithm only uses current offset information and an exponential average of the past offsets. Thus, it neither needs to store long offset history nor perform expensive computations on them. The solution provided in this paper solves problems present on IBM CCT and RADclock. We are able to achieve microsecond level accuracy without requiring any special hardware as the previous solutions. Since our protocol does not explicitly estimate the skew, which makes the implementation simpler and more robust to jitter than IBM CCT, and does not introduce offset corrections, which avoids the need of a secondary clock as in RADclock.

By looking at the synchronization problem from a new angle, this paper provides several new insights. For example, a common practice in the clock synchronization community is to avoid timing loops in the network [2, p. 3] [4, p. 16, s. 6.2]. This is because it is thought that timing loops can introduce instability as stated in [2]: *"Drawing from the experience of the telephone industry, which learned such lessons at considerable cost, the subnet topology... must never be allowed to form a loop."* Even though for some parameter values loops can

Preliminary version of this paper appears in IEEE ICNP 2013 [1].

produce instability, we show that a set of proper parameters can guarantee convergence even in the presence of loops. Furthermore, we experimentally demonstrate in Section VI that timing loops among clients can actually help reduce the jitter of the synchronization error and is therefore desirable.

The rest of the paper is organized as follows. In Section II we provide some background on how clocks are actually implemented in computers and how different protocols discipline them. Section III motivates and describes our algorithm together with an intuitive explanation of why it works. In Section IV, we analyze the convergence property of the algorithm and determine the set of parameter values and connectivity patterns under which synchronization is guaranteed. The parameter values that guarantee synchronization depend on the network topology, but there exists a subset of them that is independent of topology and therefore of great practical interest. The effect of noisy measurement and wander is studied in Section V, together with an optimization procedure that finds optimal parameter values. Experimental results evaluating the performance of the algorithm are presented in Section VI. We conclude in Section VII.

II. Computer Clocks and Synchronization

Most computer architectures keep their own estimate of time using a counter that is periodically increased by either hardware or kernel's interrupt service routines (ISRs). On Linux platforms for instance, there are usually several different clock devices that can be selected as the clock source by changing the *clocksource* kernel parameter. One particular counter that has recently been used by several clock synchronization protocols [5], [10] is the Time Stamp Counter (TSC) that counts the number of CPU cycles since the last restart of the system. For example, in the IBM BladeCenter LS21 servers, the TSC is a 64-bit counter that increments every $\delta^o = 0.416$ns since the CPU nominal frequency $f^o = 1/\delta^o = 2399.711$MHz.

Based on this counter, each server builds its own estimate $x_i(t)$ of the global time reference, UTC, denoted here by t. For example, if $c_i(t)$ denotes the counter's value of computer i at time t, then $x_i(t)$ can be computed using

$$x_i(t) = \delta^o c_i(t) + x_i^o, \tag{1}$$

where x^o is the estimate of the time when the server was turned on (t_0).

Thus, synchronizing computer clocks implies correcting $x_i(t)$ in order to match t, i.e. enforcing $x_i(t) = t$. There are two difficulties on this estimation process. Firstly, the initial time t_0 in which the counter starts its unknown. Secondly, the counter updating period δ_i ($\delta_i \approx \delta^0$) is usually unknown with enough precision and therefore presents a skew $r_i = \frac{x_i(t)-x_i(t_0)}{t-t_0}$. This is illustrated in Figure 1a where $x_i(t)$ not only increases at a different rate than t, but also starts from a value different from t_0, represented by x_i^o.

In practice, $c_i(t)$ can be approximated by a real values since the time between increments is extremely small (0.416ns) and the maximum count register value so large ($2^{64}-1$) that it would take more than 200 years to reach. Therefore, $x_i(t)$ can be described by the linear map of the global reference t, i.e.

$$x_i(t) = r_i s_i^o (t - t_0) + x_i^o, \tag{2}$$

where s_i^o is an additional skew correction implemented to compensate the skew and $r_i = \frac{\delta^o}{\delta_i}$; in Figure 1a $s_i^o = 1$. Equation (2) also shows that if one can set $s_i^o = 1/r_i$ and $x_i^o = t_0$, then we obtain a perfectly synchronized clock with $x_i(t) = t$.

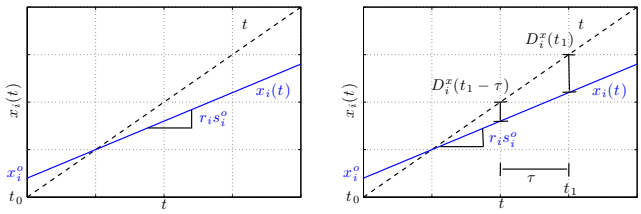

(a) Illustration of computer time estimate $x_i(t)$ and UTC time t

(b) Offset and relative skew measurements

Fig. 1: Time estimation and relative measurements

The main problem is that not only neither t_0 nor r_i can be explicitly estimated, but also r_i varies with time as shown in Figure 2a. Thus, current protocols periodically update s_i^o and x_i^o in order to keep track of the changes of r_i. These updates are made using the *offset* between the current estimate $x_i(t)$ and the global time t, i.e. $D_i^x(t) = t - x_i(t)$, and the *relative frequency error* that is computed using two offset measurements separated by τ seconds, i.e.

$$f_i^{err}(t) := \frac{D_i^x(t) - D_i^x(t-\tau)}{x_i(t) - x_i(t-\tau)} = \frac{1 - r_i s_i^o}{r_i s_i^o}. \tag{3}$$

Figure 1b provides an illustration of these measurements.

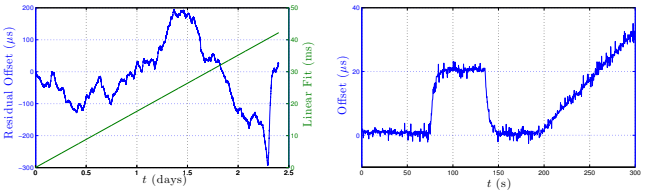

(a) Offset between two TSC counters: The straight line is a linear fit that is subtracted from the offset values in residual offset axis

(b) Example of skew and offset corrections on linux time: First a 20μs offset is added and subtracted and then a skew of 0.3ppm is introduced

Fig. 2: Comparison between two TSC counters, and skew and offset corrections using *adjtimex()*

To understand the differences between current protocols, we first rewrite the evolution of $x_i(t)$ based only on the time instants t_k in which the clock corrections are performed. We allow the skew correction s_i^o to vary over time, i.e. $s_i(t_k)$, and write $x_i(t_{k+1})$ as a function of $x_i(t_k)$. Thus, we obtain

$$x_i(t_{k+1}) = x_i(t_k) + \tau r_i s_i(t_k) + u_i^x(t_k) \tag{4a}$$
$$s_i(t_{k+1}) = s_i(t_k) + u_i^s(t_k) \tag{4b}$$

where $\tau = t_{k+1} - t_k$ is the time elapsed between adaptations; also known as poll interval [2]. The values $u_i^x(t_k)$ and $u_i^s(t_k)$ represent two different types of corrections that a given protocol chooses to do at time t_k and are usually implemented within the interval (t_k, t_{k+1}). $u_i^x(t_k)$ is usually referred to as

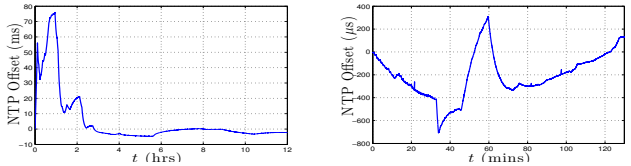

(a) NTP initialization period (b) NTP in normal regime

Fig. 3: Variations of NTP time using TSC as reference

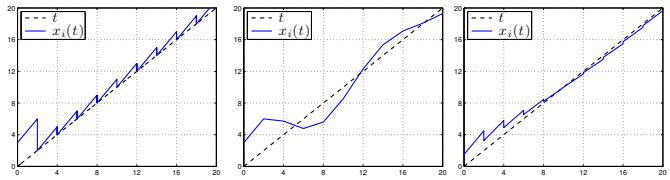

(a) Offset corrections (b) Skew corrections (c) Offset and skew corrections

Fig. 4: Current Protocols Adaptation

offset correction and $u_i^s(t_k)$ as *skew correction*.[1] See Figure 2b for an illustration of their effect on the linux time.

We now proceed to summarize the different types of adaptations implemented by current protocols. The main differences between them are whether they use offset corrections, skew corrections, or both, and whether they update using offset values $D_i^x(t_k)$, relative frequency errors $f_i^{err}(t_k)$, or both.

A. Offset corrections

These corrections consist in keeping the skew fixed and periodically introducing time changes of size $u_i^x(t_k) = \kappa_1 D_i^x(t_k)$ or $u_i^x(t_k) = \kappa_1 D_i^x(t_k) + \kappa_2 f_i^{err}(t_k)$ where $\kappa_1, \kappa_2 > 0$. They are used by NTPv3 [18] and NTPv4 [2] respectively under ordinary conditions.

These protocols have in general a slow initialization period as shown in Figure 3a. This is because the algorithm must first obtain a very accurate estimate of the initial frequency error $f_i^{err}(t_0)$. Furthermore, these updates usually generate non-smooth time evolutions as in Figures 3b and 4a, and should be done carefully since they might introduce backward jumps ($x_i(t_{k+1}) < x_i(t_k)$), which can be problematic for some applications.

B. Skew corrections

Another alternative that avoids using steep changes in time is proposed by the IBM CCT solution [10]. This alternative does not introduce any offset correction, i.e. $u_i^x(t_k) = 0$, and updates the skew $s_i(t_k)$ by $u_i^s(t_k) = \kappa_1 D_i^x(t_k) + \kappa_2 f_i^{err}(t_k)$.

The behavior of this algorithm is shown in Figure 4b. In [19] it was shown for a slightly modified version of it (used $r_i s_i(t_k) f_i^{err}(t_k)$ instead of $f_i^{err}(t_k)$) the algorithm can achieve synchronization for very diverse network architectures.

[1] These corrections can be implemented in Linux OS using the *adjtimex()* interface to update the system clock or by maintaining a virtual version of $x_i(t)$ and directly applying the corrections to it, as in IBM CCT [10] and RADclock [5]. The latter gives more control on how the corrections are implemented since it does not depend on kernel's routines.

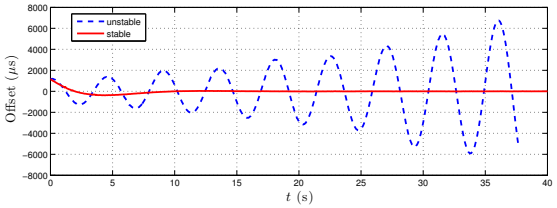

Fig. 5: Unstable clock steering using only offset information (5) and stable clock steering based on exponential average compensation (7)

However, the estimation of $f_i^{err}(t_k)$ is nontrivial as it is constantly changing with subsequent updates of $s_i(t_k)$ and it usually involves sophisticated computations [11], [12].

C. Skew and offset corrections

This type of corrections allow dependence on only offset information $D_i^x(t_k)$ as input to $u_i^x(t_k)$ and $u_i^s(t_k)$. For instance, in [6] the update $u_i^x(t_k) = \kappa_1 D_i^x(t_k)$ and $u_i^s(t_k) = \kappa_2 D_i^x(t_k)$ was proposed.

This option allows the system to achieve synchronization without any skew estimation. But the cost of achieving it, is introducing offset corrections in $x_i(t)$ as shown in Figure 4c. Therefore, it suffers from the same problems discussed in II-A.

III. Continuous Skewless Synchronization

We now present an algorithm that overcomes the limitations of the solutions described in Section II. In other words, our solution has the following two properties:

1) Continuity: The protocol does not introduce steep changes on the time value, i.e. $u_i^x(t_k) \equiv 0$.
2) Skew independence: The protocol does not use skew information $f_i^{err}(t_k)$ as input.

A solution with these properties will therefore prevent unnecessary offset corrections that produce jitter and will be more robust to noise by avoiding skew estimation. After describing and motivating our algorithm, we show how the updating rule can be implemented in the context of a network environment.

The motivation behind the proposed solution comes from trying to compensate the problem that arises when one tries to naively impose properties 1) and 2), i.e. using

$$u_i^x(t_k) = 0 \quad \text{and} \quad u_i^s(t_k) = \kappa_1 D_i^x(t_k). \tag{5}$$

Figure 5 shows that this type of clock corrections is unstable; the offset $D_i^x(t_k)$ of the slave clock oscillates with an exponentially increasing amplitude.

The oscillations in Figure 5 arise due to the fundamental limitations of using offset to update frequency. This is better seen in the continuous time version of the system (4) with (5), i.e.

$$\dot{x}_i(t) = r_i s_i(t) \text{ and } \dot{s}_i(t) = \kappa_1 D_i^x(t)$$

where $\dot{x}(t) = \frac{d}{dt}x(t)$. If we consider the offset $D_i^x = t - x_i(t)$ as the system state, then we have

$$\dot{D}_i^x = 1 - r_i s_i \text{ and } \ddot{D}_i^x = -\kappa_1 r_i D_i^x,$$

with $\ddot{x}(t) = \frac{d^2}{dt^2}x(t)$.

This is analogous to a spring mass system without friction. Thus, it has two purely imaginary eigenvalues that generate

sustained oscillations; see [7], [20] for similar examples.[2] One way to damp these oscillations in the spring-mass case is by adding *friction*. This implies adding a term that includes a frequency mismatch $f_i^{err}(t)$ in our system, which is equivalent to the protocols of Section II-B, and therefore undesired.

However, there are other ways to damp these oscillations using passivity-based techniques from control theory [21], [22]. The basic idea is to introduce an additional state y_i that generates the desired *friction* to damp the oscillations.

Inspired by [21], we consider the exponentially weighted moving average of the offset

$$y_i(t_{k+1}) = pD_i^x(t_k) + (1-p)y_i(t_k). \tag{6}$$

and update $x_i(t_k)$ and $s_i(t_k)$ using:

$$u_i^x(t_k) = 0 \quad \text{and} \quad u_i^s(t_k) = \kappa_1 D^x(t_k) - \kappa_2 y(t_k). \tag{7}$$

Figure 5 shows how the proposed strategy is able to compensate the oscillations without needing to estimate the value of $f_i^{err}(t_k)$. The stability of the algorithm will depend on how κ_1, κ_2 and p are chosen. A detailed specification of these values is given in Section IV-B.

Finally, since we are interested in studying the effect of timing loops, we move away from the client-server configuration implicitly assumed in Section II and allow mutual or cyclic interactions among nodes. The interactions between different nodes is described by a graph $G(V, E)$, where V represents the set of n nodes ($i \in V$) and E the set of *directed* edges ij; $ij \in E$ means node i can measure its offset with respect to j, $D_{ij}^x(t_k) = x_j(t_k) - x_i(t_k)$.

Within this context, a natural extension of (6)-(7) is to substitute $D_i^x(t_k)$ with the weighted average of i's neighbors offsets. Thus, we propose the following algorithm to update the clocks in the network.

Algorithm 1 (Alg1): For each computer node i in the network, perform the following actions:

- Compute the time offsets ($D_{ij}^x(t_k)$) from i to every neighbor j at time t_k.
- Update the skew $s_i(t_{k+1})$ and the moving average $y_i(t_{k+1})$ at time t_{k+1} according to:

$$s_i(t_{k+1}) = s_i(t_k) + \kappa_1 \sum_{j\in\mathcal{N}_i} \alpha_{ij} D_{ij}^x(t_k) - \kappa_2 y_i(t_k) \tag{8a}$$

$$y_i(t_{k+1}) = p \sum_{j\in\mathcal{N}_i} \alpha_{ij} D_{ij}^x(t_k) + (1-p)y_i(t_k) \tag{8b}$$

  where $\mathcal{N}_i$ represents the set of neighbors of i and the weights α_{ij} are positive.

Using this algorithm, many servers can affect the final frequency of the system. Thus, when the system synchronizes, we have

$$x_i(t_k) = r^*(t_k - t_0) + x^* \quad i \in V. \tag{9}$$

r^* and x^* are possibly different from their ideal values 1 and t_0. Their final values depend on the initial condition of all different clocks as well as the topology, which we assume to be a connected graph in this paper.

[2] In the discrete time system the oscillations increase in amplitude since there is a delay between the time the offset is measured t_k and the time the update is made t_{k+1} which makes the system unstable.

IV. Convergence Analysis

We now analyze the asymptotic behavior of system (8) and provide a necessary and sufficient condition on the parameter values that guarantee its convergence to (9). The techniques used are drawn from the control literature, e.g. [6] and [19], yet its application in our case is nontrivial.

Notation: We use $\mathbf{0}_{m\times n}$ ($\mathbf{1}_{m\times n}$) to denote the matrices of all zeros (ones) within $\mathbb{R}^{m\times n}$ and $\mathbf{0}_n$ ($\mathbf{1}_n$) to denote the column vectors of appropriate dimensions. $I_n \in \mathbb{R}^{n\times n}$ represents the identity matrix. Given a matrix $A \in \mathbb{R}^{n\times n}$ with Jordan normal form $A = PJP^{-1}$, let $n_A \leq n$ denote the total number of Jordan blocks J_l with $l \in \mathcal{I}(A) := \{1, ..., n_A\}$. We use $\mu_l(A)$, $l \in \{1, \ldots, n\}$ or just $\mu(A)$ to denote the eigenvalues of A, and order them decreasingly $|\mu_1(A)| \geq \cdots \geq |\mu_n(A)|$. Finally, A^T is the transpose of A, A_{ij} is the element of the ith row and jth column of A and a_i is the ith element of the column vector a, i.e. $a = [a_i]^T$.

It is more convenient for the analysis to use a vector form representation of (8) given by

$$z_{k+1} = Az_k \tag{10}$$

where $z_k := [x(t_k)^T s(t_k)^T y(t_k)^T]^T \in \mathbb{R}^{3n}$,

$$A := \begin{bmatrix} I_n & \tau R & \mathbf{0}_{n\times n} \\ -\kappa_1 L & I_n & -\kappa_2 I_n \\ p(-L) & \mathbf{0}_{n\times n} & (1-p)I_n \end{bmatrix} \in \mathbb{R}^{3n\times 3n},$$

$R \in \mathbb{R}^{n\times n}$ is the diagonal matrix with elements r_i and $L \in \mathbb{R}^{n\times n}$ is the Laplacian matrix associated with $G(V, E)$,

$$L_{ii} = \alpha_{ii} := \sum_{j\in\mathcal{N}_i} \alpha_{ij} \text{ and } L_{ij} = \begin{cases} -\alpha_{ij} & \text{if } ij \in E, \\ 0 & \text{otherwise.} \end{cases}$$

The convergence analysis of this section is done in two stages. First, we provide necessary and sufficient conditions for synchronization in terms of the eigenvalues of A (Section IV-A) and then use Hermite-Biehler Theorem [23] to relate these eigenvalues with the parameter values that can be directly used in practice (Section IV-B). All the proof details are included in the appendix for interested readers.

A. Asymptotic Behavior

We start by studying the asymptotic behavior of (10). That is, we are interested in finding under what conditions the series of elements $\{x_i(t_k)\}$ converge to (9) as t_k goes to infinity.

Consider the Jordan normal form [24] of

$$A := [\zeta_1 \quad \ldots \quad \zeta_{3n}]\, J\, [\eta_1 \quad \ldots \quad \eta_{3n}]^T \tag{11}$$

where $J = \text{blockdiag}(J_l)_{l\in\mathcal{I}(A)}$, ζ_i and η_i are the right and left generalized eigenvectors of A such that

$$\zeta_i^T \eta_j = \begin{cases} 1 & \text{if } j = i, \\ 0 & \text{otherwise.} \end{cases}$$

The crux of the analysis comes from understanding the relationship between the multiplicity of the eigenvalue $\mu(A) = 1$ and the eigenvalue $\mu(L) = 0$, and their corresponding eigenvectors. This is captured in the next two lemmas.

Lemma 1 (Eigenvalues of A and Multiplicity of $\mu(A) = 1$): A has an eigenvalue $\mu(A) = 1$ with multiplicity 2 if and only if the graph $G(V, E)$ is connected, $\kappa_1 \neq \kappa_2$ and $p > 0$.

Furthermore, $\mu_l(A)$ are the roots of

$$g_l(\lambda) := (\lambda - 1)^2(\lambda - 1 + p) + [(\lambda - 1)\kappa_1 + \kappa_2 - \kappa_1]\nu_l \tag{12}$$

where $\nu_l = \mu_l(\tau LR)$ and satisfies

$$\nu_n = 0 < |\nu_l| \text{ for } l \in \{1, \ldots, n-1\}. \tag{13}$$

Lemma 2 (Jordan Chains of $\mu(A) = 1$ and $\mu(A) = 1 - p$): Under the conditions of Lemma 1 the right and left Jordan chains, (ζ_1, ζ_2) and (η_2, η_1) respectively, associated with $\mu(A) = 1$ and the eigenvectors ζ_3 and η_3 associated with $\mu(A) = 1 - p$ are given by

$$[\zeta_1\ \zeta_2\ \zeta_3] = \begin{bmatrix} \mathbf{1}_n & \mathbf{1}_n & -\frac{\tau\kappa_2}{p^2}\mathbf{1}_n \\ \mathbf{0}_n & \frac{(R^{-1}\mathbf{1}_n)}{\tau} & \frac{\kappa_2}{p}R^{-1}\mathbf{1}_n \\ \mathbf{0}_n & \mathbf{0}_n & R^{-1}\mathbf{1}_n \end{bmatrix} \text{ and} \tag{14}$$

$$[\eta_1\ \eta_2\ \eta_3] = \gamma \begin{bmatrix} R^{-1}\xi & \mathbf{0}_n & \mathbf{0}_n \\ -\tau\xi & \xi & \mathbf{0}_n \\ \tau\kappa_2(\frac{1}{p} + \frac{1}{p^2})\xi & -\frac{\kappa_2}{p}\xi & \xi \end{bmatrix} \tag{15}$$

where ξ is the unique normalized left eigenvector of $\mu(L) = 0$ ($\sum_{i=1}^n \xi_i = 1$) and γ is the ξ_i-weighted harmonic mean of r_i, i.e. $\frac{1}{\gamma} = \mathbf{1}_n^T R^{-1}\xi = \sum_{i=1}^n \frac{\xi_i}{r_i}$.

The proof of Lemmas 1 and 2 can be found in Appendices A-A and A-B. We now proceed to state our main convergence result.

Theorem 1 (Convergence): The algorithm (10) achieves synchronization for any initial conditions if and only if the graph $G(V, E)$ is connected, $\kappa_1 \neq \kappa_2$, $p > 0$ and $|\mu_l(A)| < 1$ whenever $\mu_l(A) \neq 1$. Moreover, whenever the system synchronizes, we have

$$x^* = \gamma \sum_{i=1}^n \xi_i \left(\frac{1}{r_i} x_i(t_0) + \tau \frac{\kappa_2}{p^2} y_i(t_0) \right), \text{ and} \tag{16a}$$

$$r^* = \gamma \sum_{i=1}^n \xi_i (s_i(t_0) - \frac{\kappa_2}{p} y_i(t_0)). \tag{16b}$$

The proof of Theorem 1 can be found in Appendix B. Theorem 1 provides an analytical tool to understand the influence of the different nodes of the graph in the final offset x^* and frequency r^*. For example, suppose that we know that node 1 has perfect knowledge of its own frequency (r_1) and the UTC time at $t = t_0$ ($x_1(t_0) = t_0$), and configure the network such that node 1 is the unique leader like the top node in Figures 6a and 6c. It is easy to show that $\xi_1 = 1$ and $\xi_i = 0\ \forall i \neq 1$. Then, using (16a)-(16b) and definition of γ we can see that $\gamma = r_1$ and

$$x^* = x_1(t_0) + r_1\tau\frac{\kappa_2}{p^2}y_1(t_0) \text{ and } r^* = r_1 s_1(t_0) - \frac{r_1\kappa_2}{p}y_1(t_0).$$

However, since node 1 knows r_1 and t_0, it can choose $x_1(t_0) = t_0$, $s_1(t_0) = \frac{1}{r_1}$ and $y_1(t_0) = 0$. Thus, we obtain $x^* = t_0$ and $r^* = 1$ which implies by (9) that every node in the network will end up with $x_i(t) = t$. In other words, Theorem 1 allows us to understand how the information propagates and how we can guarantee that every server will converge to the desired time. Notice that the initial condition used for server 1 is equivalent to assuming that server 1 is a reliable source of UTC like an atomic clock for instance.

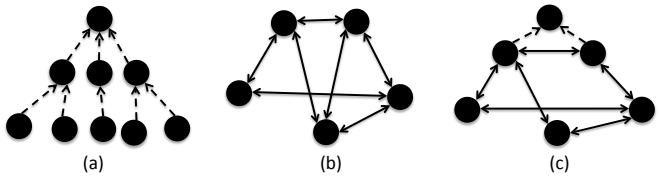

Fig. 6: Graphs with real eigenvalue Laplacians

B. Necessary and sufficient conditions for synchronization

We now provide necessary and sufficient conditions in terms of explicit parameter values (κ_1, κ_2 ,τ and p) for Theorem 1 to hold. We will restrict our attention to graphs that have Laplacian matrices with real eigenvalues. This includes for example trees (Figure 6a), symmetric graphs with $\alpha_{ij} = \alpha_{ji}$ (Figure 6b) and symmetric graphs with a leader (Figure 6c).

The proof consists on studying the Schur stability of $g_l(\lambda)$ and has several steps. We first perform a change of variable that maps the unit circle onto the left half-plane. This transforms the problem of studying the Schur stability into a Hurwitz stability problem which is solved using Hermite-Biehler Theorem which says, Given the polynomial $P(s) = a_n s^n + \ldots + a_0$, let $P^r(\omega)$ and $P^i(\omega)$ be the real and imaginary part of $P(j\omega)$, i.e. $P(j\omega) = P^r(\omega) + jP^i(\omega)$. Then $P(s)$ is a Hurwitz polynomial if and only if

1) $a_n a_{n-1} > 0$ and 2)
2) The zeros of $P^r(\omega)$ and $P^i(\omega)$ are all simple and real and interlace as ω runs from $-\infty$ to $+\infty$.

We now determine the proper parameter values that guarantee synchronization.

Theorem 2 (Parameter Values for Synchronization): Given a connected graph $G(V, E)$ such that the corresponding Laplacian matrix L has real eigenvalues. The system (10) achieves synchronization if and only if

(i) $|1 - p| < 1$ or equivalently $2 > p > 0$
(ii) $\frac{2\kappa_1}{3p} > \kappa_1 - \kappa_2 > 0$ and (iii) $\tau < \frac{p(\kappa_2 - p(\kappa_1 - \kappa_2))}{\mu_{\max}(\kappa_1 - p(\kappa_1 - \kappa_2))^2}$

where $\mu_{\max}$ is the largest eigenvalue of LR.

The proof of Theorem 2 can be found in Appendix C. Note that although $\mu_{\max}$ depends on r_i which is in general unknown, it is easy to show that $\mu_l(LR) \leq \hat{r}_{\max}\mu_l(L)$ where $\hat{r}_{\max}$ is an upper bound of the maximum rate deviation r_i. Furthermore, using Greshgorin's circle theorem, it is easy to show that $\mu_{\max}(L) \leq 2\alpha_{\max} := 2\max_i \alpha_{ii}$. Therefore, if we set

$$\tau < \frac{p(\kappa_2 - \delta\kappa p)}{2\alpha_{\max}\hat{r}_{\max}(\kappa_1 - \delta\kappa p)^2} \tag{17}$$

convergence is guaranteed for **every connected graph** with real eigenvalues.

V. Performance Optimization

We now focus on studying the performance of our algorithm in the presence of noise. We will consider two possible sources of noise corresponding to measurement errors, due to network congestion, and frequency drifts (*wander*) due to temperature variations, vibrations and interference.

Since our algorithm do not perform skew estimation the network errors only affect the offset measurements $D_{ij}^x(t_k)$ in (8). We use $g_{ij}^w w_{ij}(t_k)$ to denote the error incurred in estimating the offset between nodes i and j at time t_k.

This can be produce for instance by a congested connection between the two different nodes. We assume that $w_{ij}(t_k)$ has stationary mean $E\left[w_{ij}(t_k)\right] = \bar{w}_{ij}\ \forall t_k$ and unit variance $E[(w_{ij}(t_k) - \bar{w}_{ij})^2] = 1$ and use g_{ij}^w to weight the different connections.

On the other hand, we model the wander using a time varying rate $r_i(t_k) := r_i + \Delta r_i(t_k)$ where the drift from de mean $\Delta r_i(t_k)$ evolves according to the auto regressive process

$$\Delta r_i(t_{k+1}) = q_i \Delta r_i(t_k) + g_i^d d_i(t_k) \tag{18}$$

where q_i is the autoregression coefficient ($0 < q_i < 1$) and $d_i(t_k)$ is a random variable with zero mean $E[d_i(t_k)] = 0$ and unit variance $E[d_i(t_k)^2] = 1$. Similar models of wander has been used for instance in [12] where $d_i(t_k) \sim \mathcal{N}(0,1)$.

Equation (18) makes the evolution of $x_i(t_k)$ in (10) non-linear as now $x_i(t_{k+1}) = x_i(t_k) + \tau r_i(t_k) s_i(t_k)$. This is overcome by the fact that $\Delta r_i(t_k)$ and $\Delta s_i(t_k) := s_i(t_k) - s_i^*$ are of the order of a few parts per millions and therefore $r_i(t_{k+1}) s_i(t_{k+1})$ is approximated by

$$\begin{aligned} r_i(t_{k+1}) s_i(t_{k+1}) &\approx r_i s_i^* + \Delta r_i(t_{k+1}) s_i^* + r_i \Delta s_i(t_{k+1}) \\ &= s_i^* (q_i \Delta r_i(t_k)) + r_i (\Delta s_i(t_k) + u_i^s(t_k) + \beta_i g_i^d d_i(t_k)) \end{aligned} \tag{19}$$

where $\beta_i = \frac{s_i^*}{r_i} \approx 1$. Equation (19) also shows that we can equivalent assume that $d_i(t_k)$ is a noise source that affects $s_i(t_{k+1})$ instead of $r_i(t_{k+1})$.

This motivates the study of the stochastic process

$$z_{k+1} = A z_k + B e_k \tag{20a}$$

$$v_{k+1} = C z_k \tag{20b}$$

where $e_k = [w_k^T\ d_k^T]^T$, $B = [B_w\ B_d]$ with

$$B_w = \begin{bmatrix} \mathbf{0}_{n\times m} \\ -\kappa_1 B_G^- \mathrm{diag}[\alpha_{ij} g_{ij}^w] \\ -p B_G^- \mathrm{diag}[\alpha_{ij} g_{ij}^w] \end{bmatrix}, \quad B_d = \begin{bmatrix} \mathbf{0}_{n\times n} \\ \mathrm{diag}[\beta_i g_i^d] \\ \mathbf{0}_{n\times n} \end{bmatrix},$$

$B_G^- = \min\{B_G, \mathbf{0}_{n\times m}\}$ and B_G being the incidence matrix of $G(V,E)$ [3] and $w_k = [w_{ij}(t_k)]^T$. The matrix C maps the system state z_k to the performance metric v_k and will be specified in Section V.

In the remaining of this section, we first study the effect of biased network noise ($\bar{w}_{ij} \neq 0$) in the asymptotic frequency of the system and time offsets. In particular, we show that for arbitrarily distributed noise with stationary mean, the system's frequency tends to constantly drift unless there is a well defined leader in the topology. We then proceed to study how the parameters and network topology affect the systems performance, which is represented by the output signal v_k of the stochastic process.

We will assume that the input is white noise, i.e. $E[e_k e_l^T] = I_{m+n}\delta(l-k)$,[4] and focus on reducing the output power $||v_k||_2^2 = \lim_{N\to+\infty} \frac{1}{N} \sum_{k=0}^{N-1} v_k^T v_k$. This is known as $\mathcal{H}_2$ optimal control.

A. Frequency Drift and Time Offset

We now concentrate on studying the evolution of the first moment of the stochastic process (20). That is, we want to understand how $\bar{z}_k = E[z_k]$ evolves as $k \to +\infty$. To simplify the analysis consider the change of variable $\hat{z} = P^{-1}\bar{z} = [\eta_1\ \ \ldots\ \ \eta_{3n}]^T \bar{z}$ where P is defined as in (11). This change of variable further simplifies the dynamics of (20) giving

$$\hat{z}_{k+1} = J \hat{z}_k + P^{-1} B_w \bar{w}. \tag{21}$$

Notice that we assume we assume $\bar{d} = \mathbf{0}_n$ and thus the term $B_d \bar{d}$ is omitted from (21).

While it is difficult to provide a physical interpretation to most of the variables of the vector $\hat{z}$, it is possible to relate certain groups of states with different roles within the system. Consider the following partition of the state space $\hat{z} = [(\hat{z}^{[1,3]})^T | (\hat{z}^{[4,3n]})^T]^T$. By definition of $\hat{z}$ and (40) we have

$$\hat{z}_{k+1}^{[1,3]} = \hat{J}_1 \hat{z}_k^{[1,3]} + [\eta_1\ \eta_2\ \eta_3]^T B_w \bar{w} \tag{22}$$

$$\hat{z}_{k+1}^{[4,3n]} = \hat{J}_2 \hat{z}_k^{[4,3n]} + [\eta_4\ \ldots\ \eta_{3n}]^T B_w \bar{w} \tag{23}$$

where

$$\hat{J}_1 = \begin{bmatrix} 1 & 1 & 0 \\ 0 & 1 & 0 \\ 0 & 0 & 1-p \end{bmatrix} \text{ and } \rho(\hat{J}_2) < 1.$$

The function $\rho(A)$ is the spectral radius of A or equivalently the largest absolute value of its eigenvalues.

The following lemma is crucial in understanding the role of the different states of $\hat{z}$. Let

$$\delta\bar{x}_k := x(t_k) - \mathbf{1}_n \left(\hat{z}_1(t_k) + \hat{z}_2(t_k) - \frac{\tau\kappa_2}{p^2} \hat{z}_3(t_k) \right) \tag{24}$$

$$\delta\bar{s}_k := s(t_k) - R^{-1}\mathbf{1}_n \left(\frac{1}{\tau} \hat{z}_2(t_k) + \frac{\kappa_2}{p} \hat{z}_3(t_k) \right) \tag{25}$$

$$\delta\bar{y}_k := y(t_k) - R^{-1}\mathbf{1} \hat{z}_3(t_k). \tag{26}$$

Lemma 3 (Mean Convergence): Under the conditions of Theorem 1 the system (20) converges in mean towards

$$\delta\bar{x}_k \to \delta\bar{x}^*, \quad \delta\bar{s}_k \to \delta\bar{s}^* \text{ and } \delta\bar{y}_k \to \delta\bar{y}^*, \text{ with} \tag{27}$$

$$\delta\bar{z}^* = \left[\delta\bar{x}^{*T}\ \delta\bar{s}^{*T}\ \delta\bar{y}^{*T} \right]^T = [\zeta_4\ \ldots\ \zeta_{3n}]\, \hat{z}^{[4,3n]*} \text{ and} \tag{28}$$

$$\hat{z}^{[4,3n]*} = (I - \hat{J}_2)^{-1} [\eta_4\ \ldots\ \eta_{3n}]^T B_w \bar{w}. \tag{29}$$

The proof of Lemma 3 can be found in Appendix A-C. This result shows that while $\hat{z}^{[1,3]}$ have an homogeneous and (possibly) nonconstant effect on every node, $\hat{z}^{[4,3n]}$ in the limit introduces a fixed offset. In particular, when $\bar{w} = 0$ (e.g. zero mean noise) $\delta\bar{z}^* = 0$, $\hat{z}_2(t_k) = (\hat{z}_2)_0$, $\hat{z}_1(t_k) = (\hat{z}_1)_0 + k(\hat{z}_2)_0$ and $\hat{z}_3(t_k) \to 0$ achieving time consensus as in Theorem 1.

The next two theorems summarize the main results of this section.

Theorem 3 (Frequency Drift): In the presence of noise and under the condition of Theorem 1 the system synchronizes in mean with constant frequency if and only if

$$\sum_{i=1}^{n} \xi_i \sum_{j\in\mathcal{N}_i} \alpha_{ij} g_{ij}^w \bar{w}_{ij} = 0. \tag{30}$$

Moreover, when this happens the mean frequency r^* is given by (16b).

The proof of Theorem 3 can be found in Appendix D. Note that (30) implies that $\hat{z}_k^{[1,3]}$ behaves identically to the noiseless version. It is important to highlight the relationship between (30) and the topology of G. In particular, it is possible to differentiate two different scenarios in which (30) can be satisfied.

[3] Notice that using this definition $L = B_G^- \mathrm{diag}[\alpha_{ij}] B_G^T$

[4] $\delta(k) = 1$ if $k = 0$ and 0 o.w.

1) G has a unique leader (say $i = 1$): In this case we have $\mathcal{N}_1 = \emptyset$, i.e. $\alpha_{1j} = 0\ \forall j$, $\xi_1 = 1$ and $\xi_j = 0\ \forall j \neq 1$. That is $-\xi^T B_G^- \text{diag}[\alpha_{ij} g_{ij}^w]\bar{w} = \xi_1 0 = 0$
2) G does not have a well defined root: Thus, there are at least two nodes with $\xi_i \neq 0$ and $\bar{w}$ is such that $\xi^T B_G^- \text{diag}[\alpha_{ij} g_{ij}^w]\bar{w} = 0$.

Thus, while condition 1) can be satisfied by a proper configuration of the network, condition 2) is only satisfied by a set of values of $\bar{w}$ with zero measure. Therefore, in practice the only possible way to avoid frequency drift is by using a graph G with a well defined leader.

Furthermore, while at first sight it seems difficult to evaluate $\delta\bar{z}^*$ using (29), the following Theorem provides us with a physical interpretation.

Theorem 4 (Time Offsets): Under the conditions of Theorem 1 and (30), $\delta\bar{z}^*$ in (28) becomes

$$\delta\bar{z}^* = \begin{bmatrix} -N_1 L^\dagger B_G^- \text{diag}[\alpha_{ij}]\bar{w} \\ \mathbf{0}_n \\ \mathbf{0}_n \end{bmatrix}$$

where $L^\dagger$ is the pseudo inverse of L and $N_1 = (I_n - \gamma \mathbf{1}\xi^T R^{-1})$.

The proof can be found in Appendix E.

B. $\mathcal{H}_2$ Performance Optimization

We now proceed to study the effect of noisy measurements and wander on the output standard deviation of the system ($||v_k||_2$) when the input e_k is white noise ($E[e_k e_l^T] = I_{m+n}\delta(l-k)$). In other words, we seek to minimize

$$f(\kappa_1, \kappa_2, p, \alpha_{ij}) = ||v_k||_2 = \sqrt{E\left[\lim_{N\to+\infty} \frac{1}{N} \sum_{k=0}^{N-1} v_k^T v_k\right]}$$

Since in practice we want to avoid any frequency drift introduced by the noise we will assume in this section that (30) holds. Thus, all the randomness of the system is concentrated in $\delta x_k = N_1 x(t_k)$, $\delta s_k = N_2 s(t_k)$ and $\delta y_k = N_2 y(t_k)$ and we limit to study the stochastic process

$$\begin{aligned} \delta z_{k+1} &= NA\delta z + NBe_k \\ v_{k+1} &= C\delta z_k \end{aligned}$$

where $N = \text{blockdiag}(N_1, N_2, N_2)$.

This optimization problem is standard in the control theory community and it can be show to be equivalent to

$$\min_{X,\kappa_1,\kappa_2,p,\alpha_{ij}} \quad f(\kappa_1, \kappa_2, p, \alpha_{ij}) := \sqrt{\text{trace}[XBNN^T B^T]} \tag{31a}$$

$$\text{subject to} \quad \rho(NA) \leq \rho^* \tag{31b}$$

$$X = A^T N^T X N A + C^T C \tag{31c}$$

where A is a function of $(\kappa_1, \kappa_2, p, \alpha_{ij})$ and $\rho^* < 1$. The constrain (31b) has been added in order to maintain the stability of A.

While it is not in general easy to find the global minimum of (31) there has been intensive research in studying the continuous time [25] and discrete time [26] versions of the optimization problem

$$\min_{K,X} \quad f(K) := \sqrt{\text{trace}[X\bar{B}\bar{B}^T]} \tag{32a}$$

$$\text{subject to} \quad \rho(\bar{A}) \leq \rho^* \tag{32b}$$

$$X = \bar{A}^T X \bar{A} + \bar{C}^T \bar{C} \tag{32c}$$

where $\bar{A} := \hat{A} + \hat{B}_2 K \hat{C}_2$, $\bar{B} := \hat{B}_1 + \hat{B}_2 K \hat{D}_{21}$ and $\bar{C} := \hat{C}_1$ and δz_k is interpreted as evolving according to the closed loop standard form system

$$\begin{aligned} \delta z_{k+1} &= (\hat{A} + \hat{B}_2 K \hat{C}_2)\delta z_k + (\hat{B}_1 + \hat{B}_2 K \hat{D}_{21})e_k \\ v_k &= \hat{C}_1 \delta z_k, \end{aligned}$$

with K being the static output feedback matrix.

A few words about actually solving these optimization problems follow here. The optimization problem (31) can be written as (32) with

$$\hat{A} = N,\ \hat{C}_1 = C, \hat{C}_2 = \begin{bmatrix} B_G^T & \mathbf{0}_{m\times n} & \mathbf{0}_{m\times n} \\ \mathbf{0}_{n\times n} & I_n & \mathbf{0}_{n\times n} \\ \mathbf{0}_{n\times n} & \mathbf{0}_{n\times n} & I_n \end{bmatrix},$$

$$\hat{B}_2 = \begin{bmatrix} N_1 R & \mathbf{0}_{n\times m} & \mathbf{0}_{n\times n} & \mathbf{0}_{n\times m} & \mathbf{0}_{n\times n} \\ \mathbf{0}_{n\times n} & B_G^- & N_2 & \mathbf{0}_{n\times m} & \mathbf{0}_{n\times n} \\ \mathbf{0}_{n\times n} & \mathbf{0}_{n\times m} & \mathbf{0}_{n\times n} & B_G^- & N_2 \end{bmatrix},$$

$$\hat{B}_1 = \begin{bmatrix} \mathbf{0}_{n\times m} & \mathbf{0}_{n\times n} \\ \mathbf{0}_{n\times m} & \text{diag}[g_i^d] \\ \mathbf{0}_{n\times m} & \mathbf{0}_{n\times n} \end{bmatrix},\ \hat{D}_{21} = \begin{bmatrix} \text{diag}[g_{ij}^w] & \mathbf{0}_{m\times n} \\ \mathbf{0}_{n\times m} & \mathbf{0}_{n\times n} \\ \mathbf{0}_{n\times m} & \mathbf{0}_{n\times n} \end{bmatrix},$$

$$\text{and } K = \begin{bmatrix} \mathbf{0}_{n\times m} & \tau I_n & \mathbf{0}_{n\times n} \\ -\kappa_1 \text{diag}[\alpha_{ij}] & \mathbf{0}_{m\times n} & \mathbf{0}_{m\times n} \\ \mathbf{0}_{n\times m} & \mathbf{0}_{n\times n} & -\kappa_2 I_n \\ -p\text{diag}[\alpha_{ij}] & \mathbf{0}_{m\times n} & \mathbf{0}_{m\times n} \\ \mathbf{0}_{n\times m} & \mathbf{0}_{n\times n} & -pI_n \end{bmatrix}$$

This is the case because by definition of $\hat{B}_2$, K and $\hat{C}_2$

$$\hat{B}_2 K C_2 = \begin{bmatrix} \mathbf{0}_{n\times m} & \tau N_1 R & \mathbf{0}_{n\times n} \\ -\kappa_1 B_G^- \text{diag}[\alpha_{ij}] B_G^T & \mathbf{0}_{n\times n} & -\kappa_2 N_2 \\ -pB_G^- \text{diag}[\alpha_{ij}] B_G^T & \mathbf{0}_{n\times n} & -pN_2 \end{bmatrix}.$$

Thus, it is straight forward to see $(\hat{A} + \hat{B}_2 K \hat{C}_2) = NA$. Analogously we get $\hat{B}_1 + \hat{B}_2 K \hat{D}_{21} = NB$ and $\hat{C}_1 = C$.

The main difficulty in solving (31) in stead of (32) is that, as we showed earlier, our controller K is a nonlinear function of the parameters $K(\kappa_1, \kappa_2, p, \alpha)$ and cannot be readily obtained using (32). Furthermore, the main source of nonlinearity comes from the products $\kappa_1 \text{diag}[\alpha_{ij}]$ and $p\text{diag}[\alpha_{ij}]$. This structure is not currently supported by traditional software distributions, which usually only support sparsity patterns, and therefore needs to be implemented.

One particular package that proved to be easily adapted was Hifoo [25], [27] and more precisely in its discrete-time version Hifood [28]. These algorithms only use gradient information in their implementation of BGS and gradient bundle stages. Thus, to implement discrete time $\mathcal{H}_2$ optimization a new Matlab subroutine that evaluated the $\mathcal{H}_2$ norm f as well as its gradient was created.

The evaluation of the gradient is performed in three stages using the chain rule. We first compute the gradients of f with respect to $\bar{A} := \hat{A} + \hat{B}_2 K \hat{C}_2$, $\bar{B} := \hat{B}_1 + \hat{B}_2 K \hat{D}_{21}$ and $\bar{C} := \hat{C}_1$ which are given by

$$\nabla_{\bar{A}} f = \frac{1}{f} X \bar{A} Y, \quad \nabla_{\bar{B}} f = \frac{1}{f} X \bar{B} \quad \text{and} \quad \nabla_{\bar{C}} f = \frac{1}{f} \bar{C} Y.$$

Once $\nabla_{\bar{A}} f$, $\nabla_{\bar{B}} f$ and $\nabla_{\bar{C}} f$ are computed we can use the subroutines of hifood to compute $\frac{\partial \bar{A}}{\partial K}$, $\frac{\partial \bar{B}}{\partial K}$ and $\frac{\partial \bar{C}}{\partial K}$. Finally, we obtain

$$\nabla_{\kappa_1} f = \text{trace}\left[\left(\nabla_{\bar{A}} f^T \frac{\partial \bar{A}}{\partial K} + \nabla_{\bar{B}} f^T \frac{\partial \bar{B}}{\partial K} + \nabla_{\bar{C}} f^T \frac{\partial \bar{C}}{\partial K}\right) \frac{\partial K}{\partial \kappa_1}\right]$$

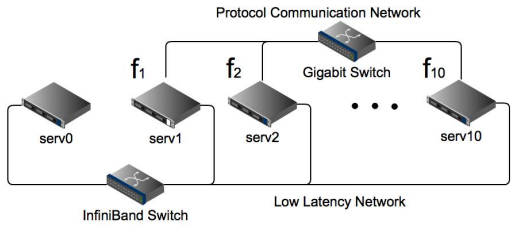

Fig. 7: Testbed of IBM BladeCenter blade servers

and similarly for other parameters.

VI. Experiments

To test our solution and analysis, we implement an asynchronous version of Algorithm 1 (Alg1) in C using the IBM CCT solution as our code base. Every node perform its own measurements and updates every τ seconds using (8), but not necessarily at the same instants t_k.

Our program reads the TSC counter directly using the `rdtsc` assembly instruction to minimize reading latencies and maintains a virtual clock that can be directly updated. The list of neighbors is read from a configuration file and whenever there is no neighbor, the program follows the local Linux clock. Finally, offset measurements are taken using an improved ping pong mechanism proposed in [10].

We run our skewless protocol in a cluster of IBM BladeCenter LS21 servers with two AMD Opteron processors of 2.40GHz, and 16GB of memory. As shown in Figure 7, the servers serv1-serv10 are used to run the protocol. The offset measurements are taken through a Gigabit Ethernet switch. Server serv0 is used as a reference node and gathers time information from the different nodes using a Cisco 4x InfiniBand Switch that supports up to 10Gbps between any two ports and up to 240Gbps of aggregate bandwidth. This minimizes the error induced by the data collecting process.

We use this testbed to validate the analysis in Section IV. First, we illustrate the effect of different parameters and analyze the effect of the network configuration on convergence (Experiment 1). Then we present a series of configurations that demonstrate how connectivity between clients is useful in reducing the jitter of a noisy clock source (Experiment 2). And finally, we compare the performance of our protocol with respect to NTP version 4 (Experiment 3) and IBM CCT (Experiment 4).

We will use several performance metrics to evaluate Alg1. The output performance signal v_k will be the vector of offset difference between the leader 1 and every other node i, i.e. $v_i(t_k) = x_i(t_k) - x_1(t_k)$ with $i \in \{2, ..., n\}$, and used a normalized version of its referred here as *mean relative deviation* , $\sqrt{S_n}$, as performance metric. In other words,

$$S_n = \frac{||v_k||_2^2}{n-1} = \frac{1}{n-1}\sum_{i=2}^{n} \langle (x_i - x_1)^2 \rangle. \qquad (33)$$

where $< \cdot >$ amounts to the sample average. We will also use the 99% Confidence Interval CI_{99} and the maximum offset (CI_{100}) as metrics of accuracy. For example, if $CI_{99} = 10\mu s$, then the 99% of the offset samples will be within $10\mu s$ of the leader.

Unless explicitly stated, the default parameter values are

$$p = 0.99, \quad \kappa_1 = 1.1, \quad \kappa_2 = 1.0 \text{ and } \alpha_{ij} = \frac{c}{|\mathcal{N}_i|}. \qquad (34)$$

The scalar c is a commit or gain factor that will allow us to compensate the effect of τ. Notice that by definition of α_{ij}, $\alpha_{ii} = c$ for every node that is not the leader.

Moreover, these values immediately satisfy (i) and (ii) of Theorem 2 since $1-p = 0.01$ and $\frac{2\kappa_1}{3p} = 0.7407 > \kappa_1 - \kappa_2 = 0.1$. The remaining condition can be satisfied by modifying τ or equivalently c. Here, we choose to fix $c = 0.7$ which makes condition (iii)

$$\tau < \frac{890.1}{\mu_{\max}} \text{ms}.$$

For fixed polling interval τ, the stability of the system depends on the value of $\mu_{\max}$, which is determined by the underlying network topology and the values of α_{ij}.

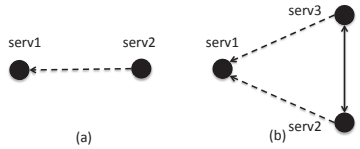

Fig. 8: Effect of topology on convergence: (a) Client-server configuration; (b) Two clients connected to server and mutually connected.

Experiment 1 (Convergence): We first consider the client server configuration described in Figure 8a with a time step $\tau = 1$s. In this configuration $\mu_{\max} \approx c = 0.7$ and therefore condition (iii) becomes $\tau < 1.2717$s. Figure 9a shows the offset between serv1 (the leader) and serv2 (the client) in microseconds. There we can see how serv2 gradually updates $s_2(t_k)$ until the offset becomes insignificant.

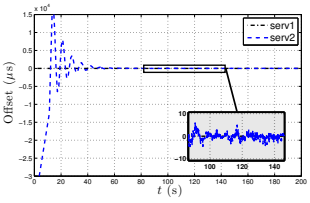

(a) Client server configuration with $\tau = 1$s. The client converges and the algorithm is stable.

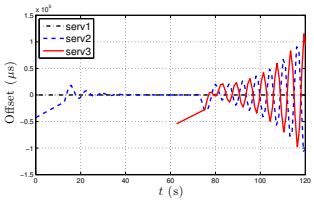

(b) Two clients mutually connected with $\tau = 1$s. The algorithm becomes unstable.

Fig. 9: Loss of stability by change in the network topology

Figure 9a tends to suggest that the set of parameters given by (34) and $\tau = 1$s are suitable for deployment on the servers. This is in fact true provided that network is a directed tree as in Figure 6a. The intuition behind this fact is that in a tree, each client connects only to one server. Thus, those connected to the leader will synchronize first and then subsequent layers will follow.

However, once loops appear in the network, there is no longer a clear dependency since two given nodes can mutually get information from each other. This type of dependency might make the algorithm unstable. Figure 9b shows an experiment with the same configuration as Figure 9a in which

serv2 synchronizes with serv1 until a third server (serv3) appears after 60s. At that moment the system is reconfigured to have the topology of Figure 8b introducing a timing loop between serv2 and serv3. This timing loop makes the system unstable.

The instability arises since after serv3 starts, the new topology has $\mu_{\max} \approx 1.5c = 1.05$. Thus, the time step condition (iii) becomes $\tau < 847.8$ms which is no longer satisfied by $\tau = 1$s.

This may be solved for the new topology (Figure 8b) by using any τ smaller than 847.8ms. However, if we want a set of parameters that is independent of the topology, we can use (17) and notice that $\alpha_{\max} = c$ and $\hat{r}_{\max} \approx 1$. We choose

$$\tau = 500\text{ms} < \frac{890.2}{2\alpha_{\max}}\text{ms} = \frac{890.2}{2c}\text{ms} = 635.9\text{ms}.$$

Figure 10 shows how now serv2 and serv3 can synchronize with serv1 after introducing this change.

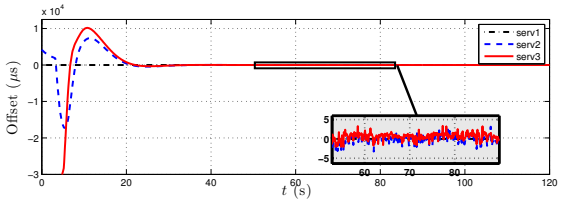

Fig. 10: Two clients mutually connected with $\tau = 500$ms

Experiment 2 (Timing Loops Effect): We now show how timing loops can be used to collectively outperform individual clients when the time source is noisy.

We run Alg1 on 10 servers (serv1 through serv10). The connection setup is described in Figure 11. Every node is directly connected unidirectionally to the leader (serv1) and bidirectionally to $2K$ additional neighbors.

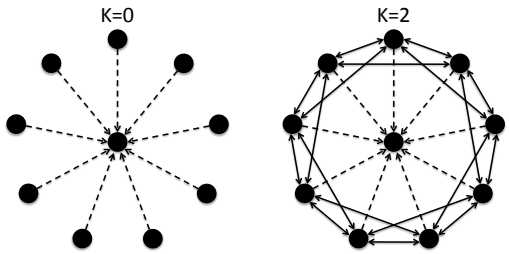

Fig. 11: Leader topologies with $2K$ neighbors connection. Connections to the leader (serv1) are unidirectional while the connections among clients (serv2 through serv10) are bidirectional

When $K = 0$ then the network reduces to a star topology and when $K = 4$ the servers serv2 through serv10 form a complete graph.

The dashed arrows in Figure 11 show the connections where jitter was introduced. To emulate a link with jitter we added random noise η with values taken uniformly from $\{0, 1, ..., \text{Jitter}_{\max}\}$ on both direction of the communication,

$$\eta \in \{0, 1, ..., \text{Jitter}_{\max}\}\text{ms}. \tag{35}$$

Notice that the arrow only shows a dependency relationship, the ping pong mechanism sends packets in both direction of the physical communication. We used a value of $\text{Jitter}_{\max} = 10$ms. Since the error was introduced in both directions of the ping pong, this is equivalent to a standard deviation of 6.05ms.

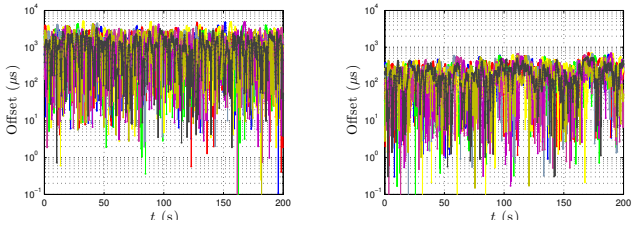

(a) Star topology ($K = 0$) (b) Complete subgraph ($K = 4$)

Fig. 12: Offset of the nine servers connected to a noisy clock source

Figure 12 illustrates the relative offset between the two extreme cases; The star topology ($K = 0$) is shown in Figure 12a, and the complete subgraph ($K = 4$) is shown in Figure 12b.

The worst case offset for $K = 0$ is $CI_{100} = 5.1$ms which is on the order of the standard deviation of the jitter. However, when $K = 4$ we obtain a worst case offset of $CI_{100} = 690.8\mu$s, an order of magnitude improvement.

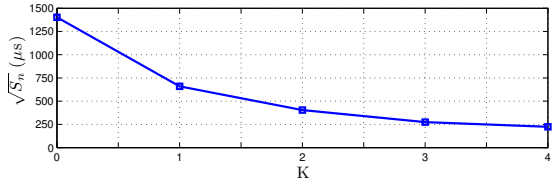

Fig. 13: Effect of the client's communication topology on the mean relative deviation. As the connectivity increases (K increases) the mean relative deviation is reduced by factor of 6.26, i.e. a noise reduction of approx. 8dB.

The change on the mean relative deviation $\sqrt{S_n}$ as the connectivity among clients increases from isolated nodes ($K = 0$) to a complete subgraph ($K = 4$) is studied in Figure 13. The results presented show that even without any offset filtering mechanism the network itself is able to perform a distributed filtering that achieves an improvement of up to a factor of 6.26 or equivalently a noise reduction of almost 8dB.

Experiment 3 (Comparison with NTPv4): We now perform a thorough comparison between our protocol (Alg1) and NTPv4. We will use the one hop configuration of Figure 8b but without the bidirectional link. Here, server serv1 is set as NTP server and as leader of Alg1, server serv2 has a client running NTPv4 and server serv3 a client running our protocol.

In order to make a fair comparison, we need both algorithms to use the same polling interval. Thus, we fix $\tau = 16$sec. This can be done for NTP by setting the parameters `minpoll` and `maxpoll` to 4 ($2^4 = 16$secs). The remainder parameter values for Alg1 are given by

$$p = 1.98, \quad \kappa_1 = 1.388 \text{ and } \kappa_2 = 1.374. \tag{36}$$

Figure 14a shows the time differences between the clients running NTPv4 and Alg1 (serv2 and serv3) , and the leader

(serv1) over a period of 30 hours. It can be seen that Alg1 is able to track serv1's clock keeping an offset smaller than 10μs for most of the time while NTPv4 incurs in larger offsets during the same period of time. This difference is produced by the fact that Alg1 is able to react more rapidly to frequency changes while NTPv4 incurs in more offset corrections that generate larger jitter.

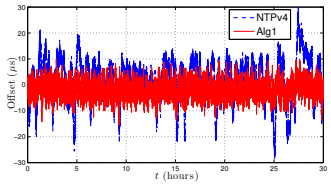

(a) Offset values of NTPv4 and Alg1 for a period of 30 hours.

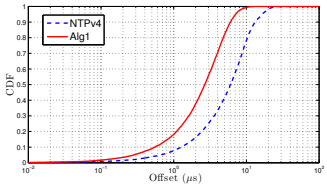

(b) Cumulative Distribution Function

Fig. 14: Performance evaluation between our solution (Alg1) and NTPv4

A more detailed and comprehensive analysis is presented in Figure 14b where we plot the Cumulative Distribution Function (CDF) of the offset samples. That is, the fraction of samples whose time offset is smaller than a specific value. Using Figure 14b we compute the corresponding 99% confidence intervals (CI_{99})

Alg1 achieves a performance of $\sqrt{S_n} = 3.1\mu$s, $CI_{99} = 9.5\mu$s and a maximum offset of $CI_{100} = 15.9\mu$s, while NTPv4 obtains $\sqrt{S_n} = 8.1\mu$s, $CI_{99} = 21.8\mu$s and a maximum offset of $CI_{100} = 28.0\mu$s. Thus, not only Alg1 achieves a reduction of $\sqrt{S_n}$ by a factor of 2.6 (-4.2dB) with respect to NTPv4, but it also obtains smaller confidence intervals and maximum offset values.

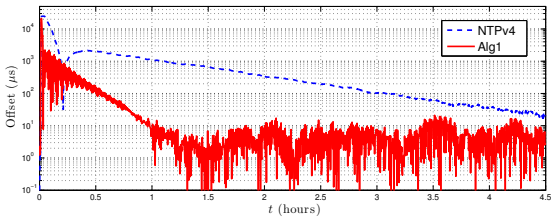

Fig. 15: Offset values of NTPv4 and Alg1 after a 25ms offset introduced in serv1.

Finally, we investigate the speed of convergence. Starting from both clients synchronized to server serv1, we introduce a 25ms offset. Figure 15 shows how Alg1 is able to converge to a $20\mu s$ range within one hour while NTPv4 needs 4.5hours to achieve the same synchronization precision.

Experiment 4 (Comparison with IBM CCT): We now proceed to compare the performance of Alg1 with respect to IBM CCT. Notice that unlike IBM CCT, our solution does not perform any previous filtering of the offset samples, the filtering is performed instead by calibrating the parameters which mostly depend on the polling interval τ chosen. Here we use $c = 0.70$, $\tau = 250ms$, $\kappa_1 = 0.1385$, $\kappa_2 = 0.1363$ and $p = 0.62$.

In Figure 16a we present the mean relative deviation $\sqrt{S_n}$ for two clients connected directly to the leader as the jitter is increased from $\text{Jitter}_{\max} = 0\mu$s (no jitter) to $\text{Jitter}_{\max} = 160\mu$s with a granularity of 1μs. The worst case offset is shown in Figure 16b. Each data point is computed using a sample run of 250 seconds.

Our algorithm consistently outperforms IBM CCT in terms of both $\sqrt{S_n}$ and worst case offset. The performance improvement is due to two reasons. Firstly, the noise filter used by the IBM CCT algorithm is tailored for noise distributions that are mostly concentrated close to zero with sporadic large errors. However, it does not work properly in cases where the distribution is more homogeneous as in this case. Secondly, by choosing $\delta\kappa = \kappa_1 - \kappa_2 = 0.002 \ll 1$ the protocol becomes very robust to offset errors.

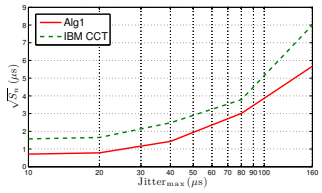

(a) Mean relative deviation $\sqrt{S_n}$

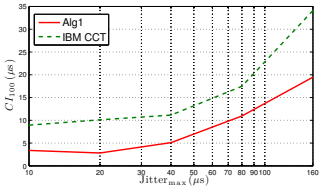

(b) Maximum offset

Fig. 16: Performance evaluation between our solution (Alg1) and IBM CCT

Experiment 5 (Frequency drift without leader): We now proceed to experimentally verify that without leader, the system tends to constantly drift the frequency. Our analysis predicts that even the minor bias in the offset measurements will produce this effect. To verify this phenomenon, we use the network topology in Figure 8b with $\tau = 0.5$s and wait for the system to converge.

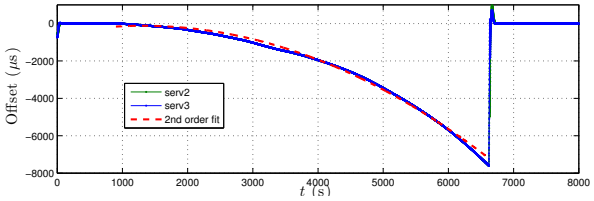

Fig. 17: Frequency drift

After 1000s the timing process of serv1 is turned off. Figure 17 shows how the offsets of serv2 and serv3 start to grow in a parabolic trajectory characteristic of a constant acceleration, i.e. constant drift. After 6600s serv1 is restarted and the system quickly recovers synchronization. A second order fit of the faulty trajectory was perform obtaining a drift of approximately -250 ns/s^2. While this is not quite significant if the first few minutes, it becomes significant as time goes on.

Experiment 6 (Jitter and Wander Tradeoff): Finally, we use the proposed $\mathcal{H}_2$ optimization scheme to show how the optimal parameter values depend on the different noise condition within the network described in Figure 18. We consider three different noise scenarios in which we either add jitter between server serv1 and servers serv2 and serv3, and/or add wander on severs serv2-serv7. In all the cases we used $\tau = 0.5$s and make offset measurements through the

InfiniBand switch to minimize the any additional source of noise.

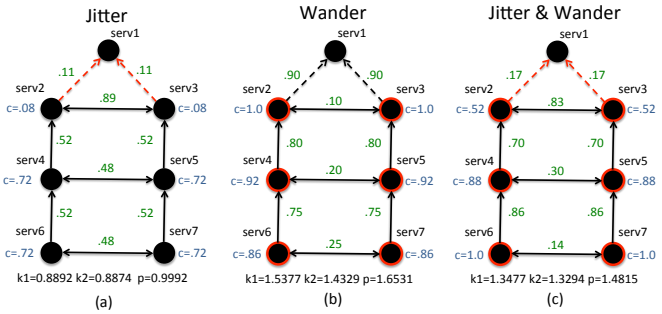

Fig. 18: Network scenarios and optimal parameters

The jitter is generated by adding in both directions of the physical communication a random value η similarly to Experiment 2 (c.f. (35)), but with a $\text{Jitter}_{\max} = 100\mu$s. This generates an aggregate offset measurement noise of zero mean and standard deviation of 40.8μs. On the other hand, the wander is generated by adding gaussian noise with zero mean and standard deviation of 0.2ppm in the $s_i(t_k)$ adaptations. As discussed in Section V, this noise can be used to emulate the wander of a bad quality clock.

We used different values of g_{ij}^w and g_i^d to differentiate the noise conditions in the optimization scheme. The large jitter scenario is represented in by $g_i^d = 1e-3\ \forall i$, $g_{21}^w = g_{31}^w = 100$ and $g_{ij}^w = 1$ otherwise. The large wander scenario is represented by $g_i^d = 1e-1\ \forall i$ and $g_{ij}^w = 1$. Finally, the large jitter and wander scenario is represented using $g_i^d = 1e-1\ \forall i$, $g_{21}^w = g_{31}^w = 100$ and $g_{ij}^w = 1$ otherwise. The output parameter values for all three cases are present also in Figure 18.

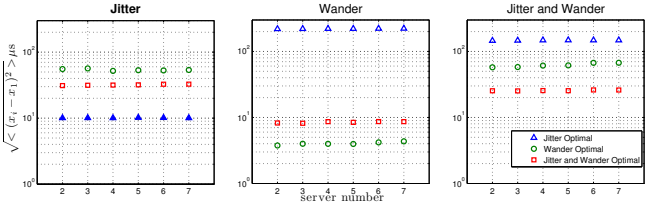

Fig. 19: $\mathcal{H}_2$ Performance optimization: offset variance vs server number

Figure 19 shows the standard deviation of the offset between servers serv2-serv7 and serv1 in the three experimental scenarios and for the three different set of parameters shown in Figure 18. It can be seen that although the configuration tuned for jitter performs very well in cases with large jitter, it performs quite poorly in scenarios with large wander. Similarly, the configuration tuned for wander does not perform well in high jitter scenarios.

However, the configuration tuned for jitter and wander is able to provide acceptable performance in all three experimental scenarios. Thus, we experimentally demonstrate a fundamental tradeoff between offset and wander.

VII. Conclusion

This paper presents a clock synchronization protocol that is able to synchronize networked nodes without explicit estimation of the clock skews and steep corrections on the time. Our solution is guaranteed to converge even in the presence of timing loops which allow different clients to share timing information and even collectively outperform individual clients when the time source has large jitter. The system is robust to noisy measurements provided that the topology has a well defined leader and we can optimize the parameter values to minimize noise variance. We implemented our solution on a cluster of IBM BladeCenter servers and empirically verified our predictions and our protocol's supremacy over several existing solutions.

References

[1] E. Mallada *et al.*, "Skewless network clock synchronization," in *ICNP. Proceedings. IEEE*, 2013.

[2] D. Mills, "Network time protocol version 4 reference and implementation guide," University of Delaware, Tech. Rep. 06-06-1, Jun. 2006.

[3] A. Sobeih *et al.*, "Almost peer-to-peer clock synchronization," *Parallel and Distributed Processing Symposium, International*, p. 21, 2007.

[4] "IEEE standard for a precision clock synchronization protocol for networked measurement and control systems," pp. 1 –269, 2008.

[5] D. Veitch, J. Ridoux, and S. B. Korada, "Robust synchronization of absolute and difference clocks over networks," *IEEE/ACM Trans. Netw.*, vol. 17, no. 2, pp. 417–430, Apr. 2009.

[6] R. Carli and S. Zampieri, "Networked clock synchronization based on second order linear consensus algorithms," in *Decision and Control (CDC), 2010 49th IEEE Conference on*, Dec. 2010, pp. 7259 –7264.

[7] E. Mallada and A. Tang, "Distributed clock synchronization: Joint frequency and phase consensus," in *Decision and Control and European Control Conference (CDC-ECC), 2011 50th IEEE Conference on*, Dec. 2011, pp. 6742 –6747.

[8] J. Ridoux, D. Veitch, and T. Broomhead, "The case for feed-forward clock synchronization," *IEEE/ACM Transactions on Networking*, vol. 20, no. 1, pp. 231–242, 2012.

[9] J. C. Corbett *et al.*, "Spanner: Google's globally-distributed database," in *Proceedings of the 10th USENIX conference on Operating Systems Design and Implementation*, ser. OSDI'12. Berkeley, CA, USA: USENIX Association, 2012, pp. 251–264. [Online]. Available: http://dl.acm.org/citation.cfm?id=2387880.2387905

[10] S. Froehlich *et al.*, "Achieving precise coordinated cluster time in a cluster environment," in *Precision Clock Synchronization for Measurement, Control and Communication, 2008. ISPCS 2008. IEEE International Symposium on*, Sep. 2008, pp. 54 –58.

[11] L. Zhang, Z. Liu, and C. Honghui Xia, "Clock synchronization algorithms for network measurements," in *INFOCOM 2002. Twenty-First Annual Joint Conference of the IEEE Computer and Communications Societies. Proceedings. IEEE*, vol. 1, 2002, pp. 160 – 169 vol.1.

[12] H. Kim, X. Ma, and B. Hamilton, "Tracking low-precision clocks with time-varying drifts using kalman filtering," *Networking, IEEE/ACM Transactions on*, vol. 20, no. 1, pp. 257 –270, Feb. 2012.

[13] J. Elson, L. Girod, and D. Estrin, "Fine-grained network time synchronization using reference broadcasts," *SIGOPS Oper. Syst. Rev.*, vol. 36, no. SI, pp. 147–163, 2002.

[14] D. Hunt, G. Korniss, and B. Szymanski, "Network synchronization in a noisy environment with time delays: Fundamental limits and tradeoffs," *Physical Review Letters*, vol. 105, no. 6, p. 068701, 2010.

[15] H. Marouani and M. R. Dagenais, "Internal clock drift estimation in computer clusters," *J. Comp. Sys., Netw., and Comm.*, vol. 2008, pp. 9:1–9:7, Jan. 2008.

[16] S. Moon, P. Skelly, and D. Towsley, "Estimation and removal of clock skew from network delay measurements," in *INFOCOM '99. Eighteenth Annual Joint Conference of the IEEE Computer and Communications Societies. Proceedings. IEEE*, vol. 1, Mar. 1999, pp. 227 –234 vol.1.

[17] M. Lemmon, J. Ganguly, and L. Xia, "Model-based clock synchronization in networks with drifting clocks," in *Dependable Computing, 2000. Proceedings. 2000 Pacific Rim International Symposium on*, 2000, pp. 177 –184.

[18] D. Mills, "Network time protocol (version 3) specification, implementation and analysis," 1992.

[19] D. Xie and S. Wang, "Consensus of second-order discrete-time multi-agent systems with fixed topology," *Journal of Mathematical Analysis and Applications*, 2011.

[20] E. Mallada and F. Paganini, "Stability of node-based multipath routing and dual congestion control," in *Decision and Control, 2008. CDC 2008. 47th IEEE Conference on*. IEEE, 2008, pp. 1398–1403.

[21] W. Ren and R. W. Beard, "Consensus algorithms for double-integrator dynamics," *Distributed Consensus in Multi-vehicle Cooperative Control: Theory and Applications*, pp. 77–104, 2008.

[22] W. Ren and R. Beard, *Distributed consensus in multi-vehicle cooperative control: theory and applications*. Springer, 2008.

[23] S. Bhattacharyya, H. Chapellat, and L. Keel, *Robust control*. Prentice-Hall Upper Saddle River, New Jersey, 1995.

[24] R. Horn and C. Johnson, *Matrix analysis*. Cambridge Univ Pr, 1990.

[25] D. Arzelier *et al.*, "H2 for HIFOO," *arXiv preprint arXiv:1010.1442*, 2010.

[26] E.-S. M. Mostafa, "Computational design of optimal discrete-time output feedback controllers," *Journal of the Operations Research Society of Japan*, vol. 51, no. 1, p. 15, 2008.

[27] S. Gumussoy *et al.*, "Multiobjective robust control with HIFOO 2.0," *arXiv:0905.3229*, May 2009.

[28] A. P. Popov, H. Werner, and M. Millstone, "Fixed-structure discrete-time controller synthesis with HIFOO," in *Decision and Control (CDC), 2010 49th IEEE Conference on*, 2010, pp. 3152–3155.

APPENDIX A
PROOF OF LEMMAS

A. Proof of Lemma 1

Proof: We first compute the characteristic polynomial

$$\det(\lambda I_{3n} - A) = \begin{vmatrix} (\lambda-1)I_n & -\tau R & \mathbf{0}_{n\times n} \\ \kappa_1 L & (\lambda-1)I_n & \kappa_2 I_n \\ pL & 0 & (\lambda-1+p)I_n \end{vmatrix}$$
$$= (\lambda-1)^n \begin{vmatrix} (\lambda-1)I_n + \frac{\tau\kappa_1}{\lambda-1}LR & \kappa_2 I_n \\ \frac{\tau p}{\lambda-1}LR & (\lambda-1+p)I_n \end{vmatrix}$$
$$= \det\big((\lambda-1)^2(\lambda-1+p)I_n + [(\lambda-1)\kappa_1 + (\kappa_2-\kappa_1)]\tau LR\big) = \prod_{l=1}^{n} g_l(\lambda),$$

where $g_l(\lambda)$ is as defined in (12) and we have iteratively use the determinant property of block matrices $\det(A) = \det(A_{11})\det(A\backslash A_{11})$ where $A = \begin{bmatrix} A_{11} & A_{12} \\ A_{21} & A_{22} \end{bmatrix}$ and $A\backslash A_{11} = A_{22} - A_{21}A_{11}^{-1}A_{12}$ is the Schur complement of A_{11} [24].

Thus, $\lambda = 1$ is a double root of the characteristic polynomial if and only if $\kappa_1 \neq \kappa_2$, $p > 0$ and τLR has a simple zero eigenvalue, i.e. (13). Now, since R is nonsingular (13) must hold for the eigenvalues of L as well, which is in fact true if and only if the directed graph $G(V, E)$ is connected [19]. ■

B. Proof of Lemma 2

Proof: We start by computing the right Jordan chain. By definition of ζ_1, $(A - I)\zeta_1 = 0_n$. Thus, if $\zeta_1 = [x^T\ s^T\ y^T]^T$, then the following system of equations must be satisfied

$$\tau Rs = \mathbf{0}_n \text{ (a)}, \ -\kappa_1 Lx - \kappa_2 y = \mathbf{0}_n \text{ (b) and}$$
$$-pLx - py = \mathbf{0}_n \text{ (c)}. \tag{37}$$

Equation (37a) implies $s = 0$. Now, since $p > 0$, (37c) implies $Lx = -y$, which when substituted in (37b) gives $(\kappa_2 - \kappa_1)y = \mathbf{0}_n$. Thus, since $\kappa_1 \neq \kappa_2$, $y = \mathbf{0}_n$ and $x \in \ker(L)$. By choosing $x = \alpha_1\mathbf{1}_n$ (for some $\alpha_1 \neq 0$) we obtain $\zeta_1 = \alpha_1 \begin{bmatrix}\mathbf{1}_n^T\ \mathbf{0}_n^T\ \mathbf{0}_n^T\end{bmatrix}^T$.

Notice that the computation also shows that ζ_1 is the unique eigenvector of $\mu(A) = 1$ which implies that there is only one Jordan block of size 2. The second member of the chain, ζ_2, and ζ_3 can be computed similarly by solving $(A - I_n)\zeta_2 = \zeta_1$ and $(A - (1-p)I_n)\zeta_3 = \mathbf{0}_n$. This gives

$$\zeta_2 = \begin{bmatrix} \alpha_2\mathbf{1}_n \\ \frac{\alpha_1}{\tau}R^{-1}\mathbf{1}_n \\ \mathbf{0}_n \end{bmatrix} \quad \text{and} \quad \zeta_3 = \alpha_3 \begin{bmatrix} -\frac{\tau\kappa_2}{p^2}\mathbf{1}_n \\ \frac{\kappa_2}{p}R^{-1}\mathbf{1}_n \\ R^{-1}\mathbf{1}_n \end{bmatrix}.$$

In computing ζ_3, we obtain $Lx = 0$ and $Rx = -\frac{\tau}{p}s = -\frac{\kappa_2\tau}{p^2}y$. ζ_3 follows by taking $y = \alpha_3 R^{-1}\mathbf{1}_n$.

The vectors η_1, η_2 and η_3 can be solved in the same way using $\eta_2^T(A-I) = \mathbf{0}_n^T$, $\eta_1^T(A-I) = \eta_2^T$ and $\eta_3^T(A-(1-p)I) = \mathbf{0}_n^T$. This gives $\eta_1 = \left[\frac{\beta_2}{\tau}R^{-1}\xi^T\ \beta_1\xi^T\ (-\frac{\kappa_2}{p}\beta_1 + \frac{\kappa_2}{p^2}\beta_2)\xi^T\right]^T$, $\eta_2 = \beta_2\left[\mathbf{0}_n^T\ \xi^T\ \frac{\kappa_2}{p}\xi^T\right]^T$ and $\eta_3 = \beta_3\left[\mathbf{0}_n^T\ \mathbf{0}_n^T\ \xi^T\right]^T$. We set $\alpha_1 = \alpha_2 = \alpha_3 = 1$; this can be done without loss of generality provided we still satisfy $\eta_l^T\zeta_l = 1$ and $\eta_l^T\zeta_h = 0$ for $l \neq h$. Finally, $\eta_1^T\zeta_1 = 1$ gives$\beta_2 = \gamma\tau$, $\eta_3^T\zeta_3 = 1$ gives $\beta_3 = \gamma$ and $\eta_1^T\zeta_2 = 0$ gives $\beta_1 = -\beta_2 = -\gamma\tau$. ■

C. Proof of Lemma 3

Proof: Since $\hat{J}_2$ has $\rho(\hat{J}_2) < 1$ then $z^{[4,3n]}(t_k)$ converges for every initial condition to a unique value which is the fix point of (23) given by $\hat{z}^{[4,3n]*}$(29) or in terms of the original system variables by $\delta\bar{z}^*$ (28).

Now by definition of $\hat{z}$, $\bar{z}_k = P\hat{z}_k = \sum_{l=1}^{3}\zeta_l\hat{z}_l(t_k) + [\zeta_4\ ...\ \zeta_{3n}]\,\hat{z}_k^{[4,3n]}$. Then, since $\hat{z}_k^{[4,3n]} \to \hat{z}_k^{[4,3n]*}$ we have

$$\bar{z}_k - \sum_{l=1}^{3}\zeta_l\hat{z}_l(t_k) \to [\zeta_4\ ...\ \zeta_{3n}]\,\hat{z}^{[4,3n]*} = \delta\bar{z}^*. \tag{38}$$

Thus, by Lemma 2 we obtain

$$\begin{bmatrix} \bar{x}_k - \delta\bar{x}^* \\ \bar{s}_k - \delta\bar{s}^* \\ \bar{y}_k - \delta\bar{y}^* \end{bmatrix} - \begin{bmatrix} \mathbf{1}_n(\hat{z}_1(t_k) + \hat{z}_2(t_k) - \frac{\tau\kappa_2}{p^2}\hat{z}_3(t_k)) \\ R^{-1}\mathbf{1}_n\left(\frac{1}{\tau}\hat{z}_2(t_k) + \frac{\kappa_2}{p}\hat{z}_3(t_k)\right) \\ R^{-1}\mathbf{1}_n\hat{z}_3(t_k) \end{bmatrix} \to \mathbf{0}_{3n}$$

which is equivalent to (27). ■

APPENDIX B
PROOF OF THEOREM 1

Proof: We first notice that whenever $x(t_k)$ approaches (9) then

$$\lim_{h\to\infty} x(t_h) - r^*\mathbf{1}_n(t_h - t_0) = x^*\mathbf{1}_n \tag{39}$$

Sufficiency: Since we are under the assumptions of Lemmas 1 and 2 we know that $\mu(A) = 1$ has multiplicity 2 and a Jordan chain of size 2. Thus, the Jordan normal form of A is

$$A = [\zeta_1 ... \zeta_{3n}] \begin{bmatrix} 1 & 1 & 0 & & \\ 0 & 1 & 0 & \mathbf{0}_{3\times 3(n-1)} & \\ 0 & 0 & 1-p & & \\ & \mathbf{0}_{3(n-1)\times 3} & & \hat{J} & \end{bmatrix} \begin{bmatrix} \eta_1{}^T \\ \vdots \\ \eta_{3n}{}^T \end{bmatrix} \tag{40}$$

where $\hat{J}$ has eigenvalues with spectral radius $\rho(\hat{J}) := \max_l |\mu_l(\hat{J})| < 1$. Thus, it follows that

$$\lim_{h\to\infty} A^h - \zeta_1\eta_1^T - (h\zeta_1+\zeta_2)\eta_2^T = \lim_{h\to\infty} [\zeta_1 ... \zeta_{3n}] \quad (41)$$
$$\begin{bmatrix} \mathbf{0}_{2\times 2} & \mathbf{0}_{2\times 1} & \mathbf{0}_{2\times(3n-2)} \\ \mathbf{0}_{1\times 2} & (1-p)^h & \\ \mathbf{0}_{(3n-2)\times 2} & & \hat{J}^h \end{bmatrix} \begin{bmatrix} \eta_1{}^T \\ \vdots \\ \eta_{3n}{}^T \end{bmatrix} = \mathbf{0}_{3n}$$

where the last equality follows since $(1-p)^h \xrightarrow[h\to\infty]{} 0$ and $\left\|\hat{J}^h\right\|_\varepsilon \le \left\|\hat{J}\right\|_\varepsilon^h \le (\rho+\varepsilon)^h \xrightarrow[h\to\infty]{} 0$, where the norm $\|\cdot\|_\varepsilon$ is chosen such that $\|A\|_\varepsilon = \rho(A) + \varepsilon$ [24, p. 297, Lemma 5.6.10] and ε is such $\rho(\hat{J}) + \varepsilon < 1$.

Right multiplying (41) with a given initial condition $z_0 = [x_0^T\ s_0^T\ y_0^T]^T$ and using (14) and (15) gives

$$\lim_{k\to\infty} x_k - (t_k - t_0)\gamma \mathbf{1}_n \xi^T (s_0 - \frac{\kappa_2}{p} y_0) = \\ = \gamma \mathbf{1}_n \xi^T (R^{-1}x_0 + \tau\frac{\kappa_2}{p^2} y_0). \quad (42)$$

Thus, equation (16) follows from identifying (42) and (39).

Necessity: The algorithm achieves synchronization whenever (39) holds. Then, it follows from (10) and (39) that asymptotically the system behaves according to

$$z_k = \begin{bmatrix} x_k \\ s_k \\ y_k \end{bmatrix} = \begin{bmatrix} x^*\mathbf{1}_n \\ r^*R^{-1}\mathbf{1}_n \\ \mathbf{0}_n \end{bmatrix} + k \begin{bmatrix} \tau r^*\mathbf{1}_n \\ \mathbf{0}_n \\ \mathbf{0}_n \end{bmatrix} \\ = (\tau r^*\zeta_2 + (x^* - \tau r^*)\zeta_1) + k r^* \tau \zeta_2.$$

Thus, since P is invertible ζ_l are linearly independent. Therefore, if the system synchronizes for arbitrary initial condition, then it must be the case that the effect of the remaining modes $\mu_l(\Gamma)$ vanishes, which can only happen if for every $\mu_l(\Gamma) \neq 1$, $|\mu_l(\Gamma)| < 1$ and the multiplicity of $\mu_l(\Gamma) = 1$ is two. Now suppose that either $\kappa_1 = \kappa_2$ or $p = 0$. Then by Lemma 1, the multiplicity of $\mu_l(\Gamma) = 1$ is not two which is a contradiction. Thus, we must have $\kappa_1 \neq \kappa_2$ and $p > 0$ whenever the system synchronizes for arbitrary initial condition. ∎

Appendix C
Proof of Theorem 2

Proof: We will show that when $G(V,E)$ is connected with $\mu(L) \in \mathbb{R}$, then (i)-(iii) are equivalent to the conditions of Theorem 1.

Since, $G(V,E)$ is connected and (i)-(ii) satisfies $p > 0$ and $\kappa_1 \neq \kappa_2$, the conditions of Lemma 1 are satisfied. Therefore the multiplicity of $\mu(A) = 1$ is two and by (13) these are the roots of $g_n(\lambda) = (\lambda-1)^2(\lambda - 1 + p)$, which corresponds to the case $\nu_n = 0$.

Thus, to satisfy Theorem 1 we need to show that the remaining eigenvalues are strictly in the unit circle. This is true for the remaining root of $g_n(\lambda)$ if and only if (i).

For the remaining $g_l(\lambda)$, this implies that are Schur polynomials. Thus, we will show that $g_l(\lambda)$ is a Schur polynomial if and only if (i)-(iii) hold. We drop the subindex l for the rest of the proof.

We first transform the Schur stability problem into a Hurwitz stability problem. Consider the change of variable $\lambda = \frac{s+1}{s-1}$. Then $|\lambda| < 1$ if and only if $\mathbb{R}[s] < 0$.

Now, since $\nu > 0$ by (13), let

$$P(s) = \frac{(s-1)^3}{\delta\kappa p\nu} g\left(\frac{s+1}{s-1}\right) = s^3 + \left(\frac{2\kappa_1}{\delta\kappa p} - 3\right)s^2 \\ + \left(\frac{4}{\delta\kappa\nu} + 3 - \frac{4\kappa_1}{\delta\kappa p}\right)s + \frac{4(2-p)}{\delta\kappa p\nu} + \frac{2\kappa_1}{\delta\kappa p} - 1$$

where $\delta\kappa = \kappa_1 - \kappa_2$.

We will apply Hermite-Biehler Theorem to $P(s)$, but first let us express what 1) and 2) of the Theorem mean here.

Condition 1) becomes

$$\frac{2\kappa_1}{\delta\kappa p} - 3 > 0. \quad (43)$$

Now let $P^r(\omega)$ and $P^i(\omega)$ be as in Hermite-Biehler Theorem, i.e. let

$$P^r(\omega) = -\left(\frac{2\kappa_1}{\delta\kappa p} - 3\right)\omega^2 + \frac{4(2-p)}{\delta\kappa p\nu} + \frac{2\kappa_1}{\delta\kappa p} - 1$$
$$P^i(\omega) = -\omega^3 + \left(\frac{4}{\delta\kappa\nu} + 3 - \frac{4\kappa_1}{\delta\kappa p}\right)\omega$$

The roots of $P^r(\omega)$ and $P^i(\omega)$ are given by $\omega_0 = \pm\sqrt{\omega_0^r}$ and $\omega_0 \in \{0,\ \pm\sqrt{\omega_0^i}\}$ respectively, where

$$\omega_0^r := \frac{\frac{4(2-p)}{\delta\kappa p\nu} + \frac{2\kappa_1}{\delta\kappa p} - 1}{\frac{2\kappa_1}{\delta\kappa p} - 3} \text{ and } \omega_0^i := \frac{4}{\delta\kappa\nu} + 3 - \frac{4\kappa_1}{\delta\kappa p} \quad (44)$$

Since the roots $P^r(\omega)$ and $P^i(\omega)$ must be real, we must have $\omega_0^r > 0$ and $\omega_0^i > 0$. Therefore, by monotonicity of the square root, the interlacing condition 2) is equivalent to

$$0 < \omega_0^r < \omega_0^i. \quad (45)$$

Thus we will show: (i)-(iii) hold $\iff$ (43) and (45) hold.

It is straightforward to see that using (i) and (ii) we can get (43). On the other hand, $\omega_o^i > 0$ from (45) together with (43) gives $0 < \frac{4}{\delta\kappa\nu} + 3 - \frac{4\kappa_1}{\delta\kappa p} < \frac{4}{\delta\kappa\nu}$, which implies that $\delta\kappa > 0$, and therefore (ii) follows.

Now using (43) and the definition of ω_0^r in (44), $\omega_0^r > 0$ becomes $\frac{4(2-p)}{\delta\kappa p\nu} + \frac{2\kappa_1}{\delta\kappa p} - 1 > 0$ which always holds under (i) and (ii) since the first term is always positive and $\frac{2\kappa_1}{\delta\kappa p} - 1 > \frac{2\kappa_1}{\delta\kappa p} - 3 > 0$ by (43).

Using (44), $\omega_0^r < \omega_0^i$ is equivalent to

$$\nu < \frac{p(\kappa_2 - \delta\kappa p)}{(\kappa_1 - \delta\kappa p)^2}. \quad (46)$$

Finally, $\nu_l = \mu_l(\tau LR) = \tau\mu_l(LR)$. Thus, since (46) should hold $\forall l \in \{1, ..., n-1\}$, then

$$\tau < \min_l \frac{p(\kappa_2 - \delta\kappa p)}{\mu_l(LR)(\kappa_1 - \delta\kappa p)^2} = \frac{p(\kappa_2 - \delta\kappa p)}{\mu_{\max}(\kappa_1 - \delta\kappa p)^2}$$

which is exactly (iii). ∎

Appendix D
Proof of Theorem 3

Proof: By Lemma 3 we know that $\bar{s}_i(t_k)$ asymptotically approaches $\delta\bar{s}_i^* + \frac{1}{\tau r_i}\hat{z}_2(t_k) + \frac{\kappa_2}{pr_i}\hat{z}_3(t_k)\ \forall i$. Therefore, $\bar{s}_i(t_k)$ becomes constant if and only if $\frac{1}{\tau r_i}\hat{z}_2(t_k) + \frac{\kappa_2}{p}\hat{z}_3(t_k)$ does.

Now from (22) it follows that

$$\begin{aligned}\hat{z}_2(t_{k+1}) &= \hat{z}_2(t_k) + \eta_2^T B_w \bar{w} \\ &= \hat{z}_2(t_k) - \tau\gamma(\kappa_1 - \kappa_2)\xi^T B_G^- \mathrm{diag}[\alpha_{ij} g_{ij}^w]\bar{w} \\ \hat{z}_3(t_{k+1}) &= (1-p)\hat{z}_3(t_k) + \eta_3^T B_w \bar{w} \\ &= (1-p)\hat{z}_3(t_k) - p\xi^T B_G^- \mathrm{diag}[\alpha_{ij} g_{ij}^w]\bar{w}.\end{aligned}$$

Thus, $z_3(t_k) \to -\xi^T B_G^- \mathrm{diag}[\alpha_{ij} g_{ij}^w]\bar{w}$ and

$$\hat{z}_2(t_k) = \hat{z}_2(0) + t_k\gamma(\kappa_2 - \kappa_1)\xi^T B_G^- \mathrm{diag}[\alpha_{ij} g_{ij}^w]\bar{w}$$

which is constant if and only if $(\kappa_2 - \kappa_1)\xi^T B_G^- \mathrm{diag}[\alpha_{ij} g_{ij}^w]\bar{w} = 0$. But since, by Theorem 1, $\kappa_1 > \kappa_2$ then we must have

$$0 = -\xi^T B_G^- \mathrm{diag}[\alpha_{ij} g_{ij}^w]\bar{w} = \sum_{i=1}^n \xi_i \sum_{j\in\mathcal{N}_i} \alpha_{ij} g_{ij}^w \bar{w}_{ij}.$$

■

Appendix E
Proof of Theorem 4

Proof: By Lemma 2 and definition of $\hat{z}$ we can compute

$$\begin{aligned}&\delta\bar{x}_k = x(t_k) - \mathbf{1}_n\left(\hat{z}_1(t_k) + \hat{z}_2(t_k) - \frac{\tau\kappa_2}{p^2}\hat{z}_3(t_k)\right) = x(t_k) \\ &-\gamma\mathbf{1}_n\left(\xi^T R^{-1}x(t_k) - \tau\xi^T s(t_k) + \tau\kappa_2\left(\frac{1}{p} + \frac{1}{p^2}\right)\xi^T y(t_k)\right) \\ &-\gamma\mathbf{1}_n\left(\tau\xi^T s(t_k) - \frac{\tau\kappa_2}{p}\xi^T y(t_k)\right) + \gamma\mathbf{1}_n\frac{\tau\kappa_2}{p^2}\xi^T y(t_k) \\ &= x(t_k) - \gamma\mathbf{1}_n\xi^T R^{-1}x(t_k) = N_1 x(t_k).\end{aligned}$$

Similarly, we have $\delta\bar{s}_k = N_2 s(t_k)$ and $\delta\bar{y}_k = N_2 y(t_k)$ where $N_2 = (I_n - \gamma R^{-1}\mathbf{1}\xi^T)$.

Moreover, since $N_1 R = R N_2$, $N_1 L = L N_2 = L$ and $N_2 B_G^- \mathrm{diag}[\alpha_{ij} g_{ij}^w]\bar{w} = B_G^- \mathrm{diag}[\alpha_{ij} g_{ij}^w]\bar{w}$ (by (30)) we have

$$\delta\bar{x}_{k+1} = \delta\bar{x}_k + \tau R\delta\bar{s}_k \tag{47a}$$

$$\delta\bar{s}_{k+1} = -\kappa_1 L\delta\bar{x}_k + \delta\bar{s}_k - \kappa_2\delta\bar{y}_k - \kappa_1 B_G^- \mathrm{diag}[\alpha_{ij} g_{ij}^w]\bar{w} \tag{47b}$$

$$\delta\bar{y}_{k+1} = -pL\delta\bar{x}_k + (1-p)\delta\bar{y}_k - pB_G^- \mathrm{diag}[\alpha_{ij} g_{ij}^w]\bar{w} \tag{47c}$$

Now, by Lemma 3 we know that (27) holds and therefore $\delta\bar{z}^*$ is a fixed point of (47). Thus, (47a) implies that $\delta\bar{s}^* = 0$ and (47b)$-\frac{\kappa_1}{p}$(47c) gives

$$(\kappa_1 - \kappa_2)\delta\bar{y}^* = 0$$

which implies $\delta\bar{y}^* = 0$ since $\kappa_1 > \kappa_2$. Finally using (47c) again we have

$$\begin{aligned}L\delta\bar{x}^* + B_G^- \mathrm{diag}[\alpha_{ij}]\bar{w} &= 0 \\ L^\dagger L\delta\bar{x}^* &= -L^\dagger B_G^- \mathrm{diag}[\alpha_{ij}]\bar{w} \\ N_3\delta\bar{x}^* &= -L^\dagger B_G^- \mathrm{diag}[\alpha_{ij}]\bar{w}\end{aligned}$$

where $N_3 = L^\dagger L = (I_n - \frac{1}{n}\mathbf{1}_n\mathbf{1}_n^T)$.

Thus, since $N_1 N_3 = N_1$ and by definition $N_1\delta\bar{x} = N_1^2\bar{x} = N_1\bar{x} = \delta\bar{x}$ it follows that

$$\begin{aligned}N_3\delta\bar{x}^* &= -L^\dagger B_G^- \mathrm{diag}[\alpha_{ij}]\bar{w} \\ N_1 N_3\delta\bar{x}^* &= -N_1 L^\dagger B_G^- \mathrm{diag}[\alpha_{ij}]\bar{w} \\ \delta\bar{x}^* &= -N_1 L^\dagger B_G^- \mathrm{diag}[\alpha_{ij}]\bar{w}\end{aligned}$$

■

Enrique Mallada (S'09-M'13)

Xiaoqiao Meng

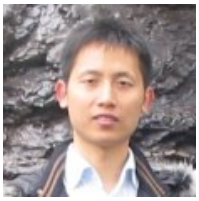

Michel Hack

Li Zhang

Ao Tang (S'01-M'07-SM'11)